

Sparse frequency LFM ladar signals

Robert V. Chimenti^{1*}, Matthew P. Dierking², Peter E. Powers^{1,3}, and Joseph W. Haus¹

¹Ladar and Optical Communications Institute and Electro-Optics Program, University of Dayton, 300 College Park, Dayton Ohio 45469-0245, USA

²Air Force Research Laboratory, AFRL_RYJM, 3109 Hobson Way, Building 622, Wright-Patterson Air Force Base, Ohio 45433-7700, USA

³Physics Department, University of Dayton, 300 College Park, Dayton Ohio 45469, USA

*Corresponding author: robchime@msn.com

Abstract: Through modeling we explored the possibility of utilizing a sparse frequency linear frequency modulation (LFM) signal for laser radar (ladar) applications. We propose a potential transmit and receive experiment utilizing the superposition of two LFM laser sources with a known difference frequency to provide the necessary segmented bandwidth. Finally we analyzed the signal performance of the proposed system showing that the range resolution of the signal can be improved by two to three times while utilizing the same modulator bandwidth as that of a continuous LFM signal.

©2009 Optical Society of America

OCIS codes: (040.2840) Heterodyne; (280.3400) Laser range finder.

References and links

1. N. Levenon and E. Mozeson, *Radar Signals*, (Wiley-Interscience, NY, 2004).
2. J. M. Senior, *Optical Fiber Communications Principles and Practice 2nd ed.*, (Prentice Hall, NJ, 1992).
3. D. S. Ly-Gagnon, S. Tsukamoto, K. Katoh, and K. Kikuchi, "Coherent Detection of Optical Quadrature Phase-Shift Keying Signals With Carrier Phase Estimation," *J. Lightwave Technol.* **24**, 12-21 (2006). <http://www.opticsinfobase.org/JLT/abstract.cfm?URI=JLT-24-1-12>.
4. M. A. Choma, C. Yang, and J. A. Izatt, "Instantaneous quadrature low-coherence interferometry with 3x3 fiber-optic couplers," *Opt. Lett.* **28**, 2162-2164 (2003). <http://www.opticsinfobase.org/ol/abstract.cfm?URI=ol-28-22-2162>.
5. C. Weidong, X. Shanxia, W. Dongjin and L. Falin, "Range Performance Analysis in Linear FMCW Radar," in 2nd International Conference on Microwave and Millimeter Wave Technology Proceedings, 654-657 (2000).
6. A.G. Stove, "Linear FMCW Radar Techniques," in *IEE Proceedings F (Radar and Signal Processing)* **139**, 343-350 (1992).
7. C. J. Karlsson and F. Å. A. Olsson, "Linearization of the Frequency Sweep of a Frequency-Modulated Continuous-Wave Semiconductor Laser Radar and the Resulting Ranging Performance," *Appl. Opt.* **38**, 3376-3386 (1999).
8. D. Nordin and K. Hyyppä, "Using a discrete thermal model to obtain a linear frequency ramping in a FMCW system," *Opt. Eng.* **44**, 74202-74205 (2005).
9. N. J. Miller, M. P. Dierking, and B. D. Duncan, "Optical sparse aperture imaging," *Appl. Opt.* **46**, 5933-5943 (2007). <http://www.opticsinfobase.org/abstract.cfm?URI=ao-46-23-5933>
10. R. L. Lucke, "Fundamentals of Wide-Field Sparse-Aperture Imaging," in 2001 IEEE Aerospace Conference Proceedings **3**, 1401-1419 (2001).
11. P. de Groot and J. McGarvey, "Chirped synthetic-wavelength interferometry," *Opt. Lett.* **17**, 1626-1628 (1992). <http://www.opticsinfobase.org/abstract.cfm?URI=ol-17-22-1626>
12. W.X. Liu, M. Lesturgie and Y.L. Lu, "Real-time sparse frequency waveform design for HFSWR system," *Electron. Lett.* **43**, 1387-1389 (2007).
13. M. J. Lindenfeld, "Sparse Frequency Transmit and Receive Waveform Design," *IEEE Trans. Aerosp. Electron. Syst.* **40**, 851-860 (2004).
14. P. M. Woodward, *Probability and Information Theory, with Applications to Radar*, (Pergamon Press, Oxford 1953).
15. J. W. Goodman, *Statistical Optics 1st ed.*, (Wiley-Interscience, 1985).

16. A. Freedman and N. Levanon, "Properties of the periodic ambiguity function," IEEE Trans. Aerosp. Electron. Syst. **30**, 938-941 (1994).
 17. B. Getz and N. Levanon, "Weight effects on the periodic ambiguity function," IEEE Trans. Aerosp. Electron. Syst. **31**, 182-193 (1995).
 18. J. W. Goodman, *Introduction to Fourier Optics 3rd ed.*, (Roberts & Company, NY, 2005).
-

1. Introduction

The range resolution of laser radar (ladar) systems is dependent on the bandwidth of the transmitted laser signal. A shorter transform limited laser pulse gives better range resolution, since range resolution is inversely proportional to signal bandwidth [1]. However, signal strength is directly proportional to pulse duration for a constant peak power, resulting in a decrease in signal to noise ratio (SNR) with decreasing pulse width. Reconciling these two opposing trends are well established and are major driving forces behind modern ranging detection technology.

Ladar systems can benefit greatly by utilizing techniques developed by the radar community. Many of the same issues faced by radar systems are the same for ladar. A particularly successful radar technique for ranging uses frequency chirped signals [1]. The long duration of the chirped signal is advantageous from the standpoint of signal strength and therefore improving the SNR. For this reason chirped signals, which have the advantage of increasing the bandwidth of the signal while maintaining relatively large pulse durations, have become the most popular form of radar signals [1].

Borrowing this technique directly from the radar community and applying it towards ladar systems is not entirely possible. In radar systems the receiver directly measures the electric field whereas in ladar systems a simple, direct field measurement is not possible. To overcome this obstacle most ladar receivers utilize either homodyne or heterodyne mixing [2]. Recent work in ladar signals has also utilized in-phase and quadrature (I/Q) detection in order to determine the complex envelope of the signal [3, 4]. A powerful technique to determine the range from the homodyne or heterodyne signal is to digitally correlate the signal with a matched filter to determine the range [1].

The most common chirped signal has a time dependence given by $\exp[i(\alpha t + \beta t^2/2)]$. Since frequency is the derivative of phase, a quadratic phase waveform will result in a linear frequency chirp, or has a linear frequency modulation (LFM) in time. While this technique is relatively well developed in the radar community [1, 5, 6], LFM signal generators for ladar applications have the potential to be even better since the higher optical frequencies can handle much larger (higher bandwidth) LFM chirps. However, the ladar approach will only compete with radar if the LFM chirp is larger than those obtained for radar. Obtaining large frequency chirps of the order of 1 GHz on time scales of 1 μ s are technologically challenging.

Even though the basic physics is similar for radar and ladar, there are appreciable differences in the transmitter and receiver designs. One major hurdle in the application of LFM laser signals is the production of the signal itself. It is important that the signal maintain a linear frequency ramp or chirp over the entire modulation range. For small LFM chirps this is not an issue but as the chirp bandwidth increases it becomes difficult to maintain linearity. There are many different modulation techniques used to generate LFM signals. For example the frequency can be modified through the laser source by modulating the cavity length, temperature, or drive current. The internal cavity modulation schemes can generate large frequency chirps. External laser cavity modulations schemes such as using electro-optic (EO) and acousto-optic (AO) modulators provide better control. While these schemes typically have a smaller chirp bandwidth, the linearity of the frequency chirps can be better maintained. It remains technically challenging to sustain linearity over relatively large spans of time [7, 8].

In order to overcome this problem we take a cue from the sparse aperture imaging [9, 10], chirped synthetic-wavelength interferometry [11], and sparse frequency radar [12, 13] communities by using two wavelength shifted coherent sources that each have a continuous wave LFM (CW-LFM) imposed on them. In this paper we analyze the processing of these signals and analyze the improvement in range resolution.

2. Sparse Frequency LFM Signal

2.1. Signal Generation

To produce a sparse frequency LFM chirped signal we start with two frequency and phase stabilized lasers with a known difference frequency (df). The two lasers are combined in a single optical fiber and transmitted through a frequency modulator via a fiber optic coupler, assuring that any resultant noise from the modulator is correlated in both chirped signals. It is assumed that the frequency modulator is an acousto-optic modulator which has a frequency offset, f_o in addition to the frequency shift. The modulator will periodically linearly shift the frequency of the lasers from f_o to $f_o + B$, where f_o is the fundamental frequency shift of the modulator that will later allow for heterodyne mixing, and B is the chirp bandwidth. Fig. 1 shows a frequency spectrum of the resultant waveform.

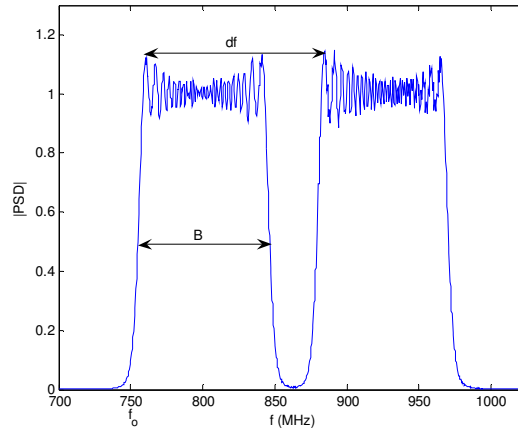


Fig. 1. Normalized power spectral density (PSD) of sparse frequency LFM signal.

The modulated laser beam is sent to a target and the returned scattered light is collected and mixed with one of the unchirped laser signals, which is used as a local oscillator (LO). The mixed signals are detected through an I/Q detection assembly. A schematic for the proposed experiment is shown in Fig 2. The I/Q detection scheme allows the retrieval of the complex envelope which can be correlated with a matched filter to determine the range and range resolution.

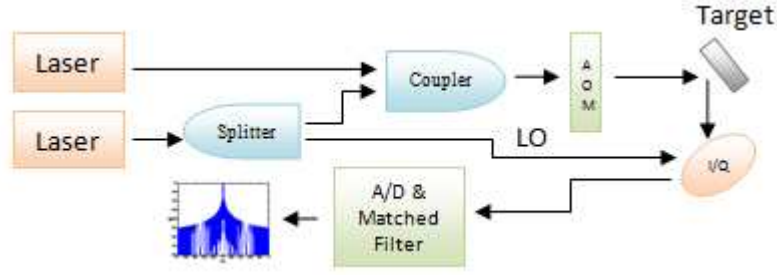


Fig. 2. Schematic setup for sparse frequency LFM chirped signal generation, detection and processing.

2.2. Field on the detector

Given the basic transmit and receive setup as described above and shown in Fig. 2, the resultant heterodyned signal can be determined by looking at the total field on the detector and the current it generates, which is proportional to the magnitude squared of the field, given by

$$s(t) \Big|_0^T = \left| \tilde{A}_1 e^{i\left(2\pi(f+f_o)t + \frac{1}{2}\beta t^2\right)} + \tilde{A}_2 e^{i\left(2\pi(f+f_o+df)t + \frac{1}{2}\beta t^2\right)} + \tilde{A}_{LO} e^{i2\pi f t} \right|^2, \quad (1)$$

where \tilde{A}_1 and \tilde{A}_2 are the complex amplitudes of the fields returning from the target and \tilde{A}_{LO} is the complex amplitude of the local oscillator. Since the field amplitudes of the two are approximately equal, $\tilde{A}_1 \approx \tilde{A}_2 = \tilde{A}$ and are much less than the field amplitude of the LO, Eq. (1) can be simplified to Eq. (2)

$$s(t) \Big|_0^T \approx I_{LO} + \left[\tilde{A} \tilde{A}_{LO}^* e^{i\left(2\pi f_o t + \frac{1}{2}\beta t^2\right)} + \tilde{A} \tilde{A}_{LO}^* e^{i\left(2\pi(f_o+df)t + \frac{1}{2}\beta t^2\right)} + c.c. \right], \quad (2)$$

where *c.c.* represents the complex conjugate of the first two terms inside of the brackets. Utilizing I/Q detection the complex amplitude in the brackets of Eq. (2) can be extracted. The complex signal is given by

$$u(t) \Big|_0^T \approx \tilde{A} \tilde{A}_{LO}^* \left[e^{i\left(2\pi f_o t + \frac{1}{2}\beta t^2\right)} + e^{i\left(2\pi(f_o+df)t + \frac{1}{2}\beta t^2\right)} \right]. \quad (3)$$

The signal is captured with a digitizer and the range resolution information is extracted by applying a matched filter processing technique.

2.3. Ambiguity function

The range and Doppler resolution of the signal can be analyzed using the ambiguity function introduced by Woodward in 1953 [14], defined by

$$|\chi(\tau, \nu)| = \left| \int_{-\infty}^{\infty} u(t) u^*(t + \tau) e^{i2\pi\nu t} dt \right|, \quad (4)$$

which was developed based on matched filter processing. Eq. (4) provides an understanding of the ambiguity in both time delay (τ) and Doppler shift (ν). For the sake of this investigation stationary targets are assumed so $\nu = 0$ and Eq. (4) simply reduces to the autocorrelation of the complex envelope. In order to derive an analytic solution for range ambiguity we will assume that the field amplitudes are slowly varying, and then utilize the Wiener-Khinchin theorem to calculate the autocorrelation of the signal. The Wiener-Khinchin theorem states that the Fourier transform of the PSD is equal to the auto-correlation of the signal [15]. Since it has been shown that the ambiguity function of a periodic function (e.g. CW-LFM signal) is equal to the ambiguity function of a single pulse multiplied by a function which is only dependant on ν , and that this function reduces to unity when $\nu = 0$ [1, 16, 17], in this case it is only necessary to look at the ambiguity function of a single pulse. Therefore the PSD is $|U(f)|^2/T$ where $U(f)$ is the Fourier transform of Eq. (3). Calculating $U(f)$ is straightforward by completing the square in the exponent and assuming that $u(t)$ is periodic with period T .

$$U(f) = \tilde{A} \tilde{A}_{LO}^* \left\{ \sqrt{\frac{\pi}{\beta}} e^{i\frac{2\pi^2}{\beta}(f-f_o)^2} \sqrt{\frac{\pi}{\beta}} \left(T - \frac{\pi}{\beta}(f-f_o) \right) \int_{\sqrt{\frac{\pi}{\beta}}(f-f_o)}^{\sqrt{\frac{\pi}{\beta}} \left(T - \frac{\pi}{\beta}(f-f_o) \right)} e^{i\frac{\pi}{2}u^2} du \right. \\ \left. + \sqrt{\frac{\pi}{\beta}} e^{i\frac{2\pi^2}{\beta}(f-f_o-df)^2} \sqrt{\frac{\pi}{\beta}} \left(T - \frac{\pi}{\beta}(f-f_o-df) \right) \int_{\sqrt{\frac{\pi}{\beta}}(f_o+df-f)}^{\sqrt{\frac{\pi}{\beta}} \left(T - \frac{\pi}{\beta}(f-f_o-df) \right)} e^{i\frac{\pi}{2}u^2} du \right\}. \quad (5)$$

Solutions to Eq. (5) can be evaluated numerically [16]. In order to derive an analytic solution we recognize that the Fourier transform of a chirped exponential can be approximated by a rectangle function in frequency space. Under this approximation, Eq. (5) becomes:

$$U(f) \approx \tilde{A} \tilde{A}_{LO}^* \left\{ \sqrt{i\frac{2\pi}{\beta}} e^{i\frac{2\pi^2}{\beta}(f-f_o)^2} \text{rect} \left(\frac{f - \left(f_o + \frac{B}{2} \right)}{B} \right) + \sqrt{i\frac{2\pi}{\beta}} e^{i\frac{2\pi^2}{\beta}(f-f_o-df)^2} \text{rect} \left(\frac{f - \left(f_o + df + \frac{B}{2} \right)}{B} \right) \right\}. \quad (6)$$

The PSD is found from Eq. (6) by taking the modulus squared and dividing by the period, which simplifies to:

$$PSD_U(f) = \frac{I \times I_{LO}}{B} \left[\text{rect} \left(\frac{f - \left(f_o + \frac{B}{2} \right)}{B} \right) + \text{rect} \left(\frac{f - \left(f_o + df + \frac{B}{2} \right)}{B} \right) \right] \\ + 2 \cos \left(\frac{2\pi T df}{B} f - \frac{\pi T df}{B} (2f_o + df) \right)$$

$$\times \left[\begin{array}{l} \text{rect} \left(\frac{f - \left(f_o + \frac{B-df}{2} \right)}{B} \right), \quad \text{if } df \leq B \\ 0, \quad \text{if } df > B \end{array} \right] \quad (7)$$

Next we Fourier transform Eq. (7) to get the auto-correlation of $u(t)$ and thus the range ambiguity of the signal.

$$\begin{aligned} |\chi(\tau)| &= I \times I_{LO} \left| \text{sinc}(B\tau) e^{-i2\pi \left(f_o + \frac{B}{2} \right) \tau} \left(1 + e^{-i2\pi df \tau} \right) + \right. \\ &\quad \left. \frac{B-df}{B} \left[\delta \left(\tau + \frac{Tdf}{B} \right) + \delta \left(\tau - \frac{Tdf}{B} \right) \right] e^{-i \frac{2\pi^2 df}{B} (df+2f_o)\tau} \right. \\ &\quad \left. \otimes \left[\begin{array}{l} \text{sinc}((B-df)\tau) e^{-i2\pi \left(f_o + \frac{B+df}{2} \right) \tau}, \quad \text{if } df \leq B \\ 0, \quad \text{if } df > B \end{array} \right] \right|. \end{aligned} \quad (8)$$

Inspection of Eq. (8) shows that the ambiguity function has a central peak at $\tau = 0$ as would be expected from a LFM signal. But, due to frequency interference there are also two other peaks located at $\tau = \pm(T \times df)/B$ which decrease as the frequency components of the two chirps pull apart and eventually disappear when their frequency contents are completely uncorrelated. The most interesting result of Eq. (8) comes from the phase term $(1 + e^{-i2\pi df \tau})$ multiplying the sinc function in the first term. This phase is due to the superposition of the two waveforms resulting in a narrowing of the central peak at $\tau = 0$ as df increases, as would be expected given that the overall bandwidth is increasing. It is interesting to note that the linewidth narrowing behaves in the same manner as increasing the separation in sparse aperture imaging which narrows the central peak of the point spread function (PSF). The linewidth narrowing comes at a cost as seen by the addition of side lobes on the ambiguity function. This is analogous to sparse aperture imaging where as the central peak narrows the energy is pushed into the wings therefore raising the side lobes and increasing the peak to side lobe ratio (PSLR). Note that in radar/ladar imaging the PSLR is a measure of the maximum amount of energy in the ghost images therefore a lower PSLR is desirable.

2.4. Results

To verify Eq. (8) we developed a numerical model to perform the autocorrelation of Eq. (3). The output was then normalized and converted to decibels generating $|\chi(\tau)|$. When the numerical model was compared to the normalized approximated analytical solution they matched extremely well. For most difference frequencies the two plots matched to within less than one percent at the central lobe. Fig. 3 shows the numerical and analytical solutions plotted together for a time bandwidth product of 100 and a 50MHz difference frequency.

Utilizing the analytical model allows us to understand the underlying physical properties of the range ambiguity as shown in the previous section. Although the analytic model is in good agreement with the numerical model, for determining specific details of performance of the range resolution and the PSLR, the numerical model is more accurate. We programmed an algorithm to record the full width at half maximum (FWHM) (-3dB) of the central lobe ($\delta\tau$) as well as the PSLR as the simulation stepped through 1MHz difference frequency increments. The PSLR is defined as the ratio of the largest side lobe to the main peak. The relationship between range resolution and the FWHM of the central lobe is given by

$$\delta R = \frac{\delta \tau \times c}{2} \quad (9)$$

By making use of the relationship in Eq. (9) the range resolution (δR) as a function of difference frequency can be recorded, as shown in Fig. 4. Figure 4 shows the PSLR and δR for the sparse frequency LFM signal with $B = 100\text{MHz}$, $T = 1\mu\text{s}$, $f_0 = 750\text{MHz}$ as a function of df . Also shown in Fig. 4 is the result for a continuous frequency LFM signal with the same period, frequency offset and equivalent bandwidth ($df+B$) for comparison.

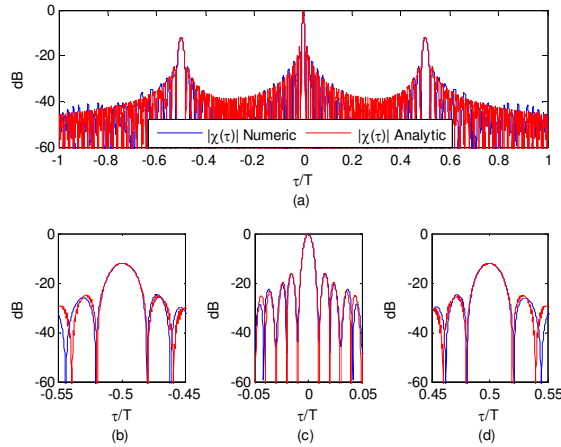


Fig. 3. Comparison of numeric and analytic representation of the ambiguity function. (a) Full range, (b) Left peak, (c) Center peak, (d) Right peak.

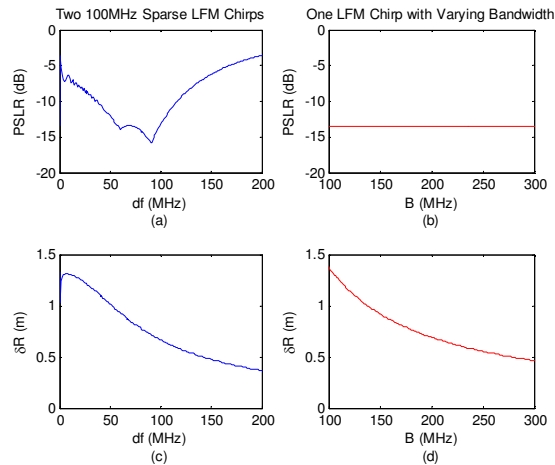


Fig. 4. (a) PSLR of sparse frequency LFM chirped signal, (b) PSLR of standard LFM chirp signal, (c) Range resolution of the sparse frequency LFM chirped signal, (d) Range resolution of a standard LFM chirp signal.

From Fig. 4 the range resolution of the sparse frequency LFM signal is approximately the same as the continuously chirped signal with twice the chirp bandwidth on the carrier signal. The only significant difference between the two signals is the PSLR, which as discussed

earlier are due to the energy in the central peak being redistributed to the side lobes. Continuing our investigation of this signal as a function of difference frequency we constructed a function by taking the modulus of the autocorrelation function with difference frequency (df) now plotted as a variable. It enables a visualization of how df affects the range ambiguity. Figure 5. shows the additional bands of ambiguity located at $\tau = \pm(T \times df)/B$ which tend to spread out and decrease in intensity as df is increased.

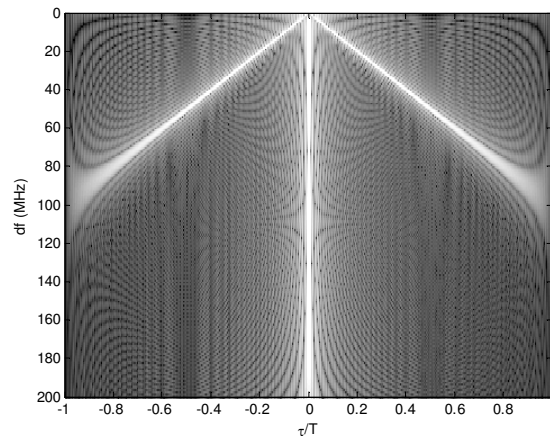


Fig. 5. Autocorrelation function (dB) plotted versus difference frequency.

3. Conclusion and Outlook

The two chirped sparse frequency model shows an advantage of increasing range resolution without the need for additional chirped frequency bandwidth. We have also shown that interference in the frequency domain will create bands of additional ambiguity, when the difference frequency is less than the chirp bandwidth. After reviewing all of the simulation data we conclude that this type of waveform has the potential to increase the range resolution by two to three times for the same chirped bandwidth depending on the PSLR requirements of the application of lidar systems without sacrificing signal strength. An initial investigation into expanding the scope for this type of signal into N superimposed waveforms has shown promise and we plan to further investigate their potential in the near future. We are currently developing an experiment to verify the results of this model.

Acknowledgments

This effort was supported in part by the U.S. Air Force through contract number FA8650-06-2-1081, and the University of Dayton Ladar and Optical Communications Institute (LOCI). The authors would like to extend special thanks to Nicholas Miller, Bradley Duncan, Igor Anisimov, and everyone else at LOCI for their help and support. The views expressed in this article are those of the authors and do not reflect on the official policy of the Air Force, Department of Defense or the U.S. Government.